Published in final edited form as:
J Control Release. 2007 October 8; 122(3): 269–277. doi:10.1016/j.jconrel.2007.06.016.

Polymer Platforms for Drug Delivery and Biomedical Imaging

Zheng-Rong Lu, **Furong Ye**, and **Anagha Vaidya**
Department of Pharmaceutics and Pharmaceutical Chemistry, University of Utah, Salt Lake City, Utah 84108

Abstract

Biocompatible synthetic polymers have demonstrated advantageous pharmacokinetic properties as compared to small molecular agents. Incorporation of low molecular weight therapeutics and imaging agents into biocompatible polymers can optimize their pharmacokinetic properties with improved efficacy of therapy and diagnostic imaging, respectively. We have applied the concept of drug delivery to design safe and effective contrast agents for magnetic resonance imaging (MRI) and used biomedical imaging in non-invasive evaluation of drug delivery and image-guided therapy. We summarize here the recent progress in our research on biodegradable macromolecular MRI contrast agents, non-invasive visualization of in vivo drug delivery of polymeric conjugates with contrast enhanced MRI, and contrast enhanced MRI guided photodynamic therapy. The preliminary results have shown that biocompatible polymers can be used as an effective platform for drug delivery and biomedical imaging. Safe and effective imaging agents can be designed by using the concept of polymeric drug delivery. Biomedical imaging can be used as a non-invasive method for the evaluation of in vivo drug delivery of polymeric drug delivery systems. The combination of drug delivery and biomedical imaging can result in image-guided therapies, which include tumor detection, therapy and non-invasive evaluation of therapeutic responses.

Biocompatible and water-soluble polymers have demonstrated unique pharmacokinetic properties, including prolonged blood circulation and tissue retention, and preferential accumulation in lesions with blood vessel hyperpermeability, because of their large sizes. Biocompatible synthetic polymers have been used as a platform for the modification of pharmacokinetics of small molecular therapeutics and imaging agents to improve their efficacy in drug delivery and molecular imaging [1,2]. The conjugation of therapeutics to biocompatible polymers prolongs in vivo drug retention time, increases drug bioavailability, reduces systemic toxicity and enhances therapeutic efficacy [3,4]. The incorporation of imaging agents into biocompatible polymers prolongs their retention in the tissues of interest with increased concentrations, which allows more accurate disease detection and characterization [5,6]. For example, the incorporation of a magnetic resonance imaging (MRI) contrast agent into a macromolecule would increase its blood circulation time for effective contrast enhanced cardiovascular imaging and tumor imaging [7,8].

Both drug delivery and molecular imaging can benefit from the large sizes and unique pharmacokinetic properties of biomedical polymers. However, the applications of biomedical polymers in these areas are not mutually exclusive. In fact, the concept of drug delivery can be applied in molecular imaging to design and develop effective and specific imaging agents

Correspondence to: Dr. Zheng-Rong Lu, 421 Wakara Way, Suite 318, Salt Lake City, UT 84108, Phone: 801 587-9450, Fax: 801 585-3614, Email: E-mail: zhengrong.lu@utah.edu.

and probes. Molecular imaging provides a non-invasive tool for visualization of real-time pharmacokinetics of polymeric drug delivery systems after labeling with appropriate imaging agents or probes [9,10], which can unveil the complicated mechanisms of in vivo drug delivery and its correlation to pharmacodynamics. Thus, the combination of drug delivery and molecular imaging on the same polymer platform will result in more effective therapeutic regimens—image-guided therapies, which include earlier and more accurate diagnosis, efficacious treatment, rapid and non-invasive assessment of responses to the therapies, and personalized patient care.

The applications of biomedical polymers in drug delivery and molecular imaging are broad and comprehensive. Various polymeric drug delivery systems have been previously reviewed in numerous publications [1,3,11–13]. Polymers have been used in the design and development of novel imaging agents for various imaging modalities, including computed tomography (CT) [14], MRI [5], single photon emission computed tomography (SPECT) [15], positron emission tomography (PET) [16], ultrasound [17] and optical imaging [18]. We summarize here our recent research progress using biomedical polymers as a platform for both drug delivery and molecular imaging, including biodegradable macromolecular MRI contrast agents; non-invasive visualization of in vivo drug delivery of polymeric conjugates with contrast enhanced MRI; and bifunctional polymeric conjugates for image-guided photodynamic therapy.

1. Polymer Gd(III) chelate conjugates with a disulfide spacer as biodegradable macromolecular MRI contrast agents

Magnetic resonance imaging (MRI) is a non-ionization imaging modality, which relies on the difference in the longitudinal or transverse relaxation rates ($1/T_1$ or $1/T_2$) of water nuclei (mainly protons) of different tissues [19]. MRI provides three-dimensional, high-resolution images of soft tissues. In many cases, a contrast agent is used to enhance the image contrast between normal tissue and diseased tissue for accurate diagnosis. MRI contrast agents are paramagnetic metal chelates, e.g. Gd(III), Fe(III) and Mn(II) complexes, and ultrasmall supermagnetic iron oxide, which are able to alter the relaxation rate of the surrounding water protons, resulting in image contrast enhancement [20]. Clinically available MRI contrast agents are mostly low molecular weight Gd(III) chelates, including Gd-DTPA, Gd-DOTA and their derivatives. These agents have a transient plasma retention time and cannot effectively differentiate diseased tissue from normal tissues. These low molecular weight contrast agents have been incorporated into biomedical polymers to modify their pharmacokinetics, thus improving the image contrast enhancement. [2,5,7,8].

Although these macromolecular contrast agents have demonstrated superior efficacy in cardiovascular and cancer MR imaging in preclinical studies, their clinical development is limited because of potential toxicity related to their slow excretion. Toxicity of an imaging agent is much more problematic in biomedical imaging than that of an anti-cancer agent in drug delivery. The strategy of drug delivery is to maintain anticancer drugs in tumor tissue for a sufficiently prolonged period at an efficacious concentration. This strategy may not be suitable for the design and development of imaging agents and probes, supposedly because they should not have any pharmacological effects. Gd(III) ions are highly toxic and long-term tissue retention of macromolecular MRI contrast agents may result in release of toxic Gd(III) ions due to metabolism. Various macromolecular MRI contrast agents have been prepared by conjugating the gadolinium chelates to the biodegradable macromolecules, including polyamino acids [21], polysaccharides [22] and proteins [23]. However, biodegradation of these biomedical polymers is an enzymatic process that mainly occurs in cellular lysosomal compartments. Since MRI contrast agents are extracellular agents, degradation and excretion of macromolecular MRI contrast agents based on these biodegradable polymers are still too slow for clinical development.

We have recently introduced a biodegradable disulfide spacer in the polymer Gd(III) chelate conjugates to develop a novel class of biodegradable macromolecular MRI contrast agents with rapid excretion of Gd(III) chelates. Literature suggests that the disulfide spacer can be gradually cleaved in the plasma by the endogenous thiols including cysteine and glutathione (reduced form) via thiol-disulfide exchange reaction [24]. However, the *in vivo* degradation of the disulfide bonds is much more complicated than mere thiol-disulfide exchange reaction. The cleavage of the disulfide spacer might also involve enzymatic and oxidative reactions because of high oxygen concentration in the blood plasma. Further studies are required to unravel the detailed degradation mechanism of the disulfide spacer. Nonetheless, the disulfide spacer resulted in the rapid excretion of Gd(III) chelates of a prototype biodegradable macromolecular MRI agent, poly(*L*-glutamic acid)-cystamine-(Gd-DO3A), in an animal model as compared to a corresponding conjugate with a non-degradable spacer [25].

Poly(*L*-glutamic acid)-cystamine-(Gd-DO3A) demonstrated strong contrast enhancement in the blood and tumor, but excreted more rapidly than poly(*L*-glutamic acid)-1,6-hexanediamine-(Gd-DO3A) a polymer conjugate with non-degradable spacer [25]. Figure 1 shows the three dimensional maximum intensity projection (3D MIP) MR images of mice bearing MDA-MB-231 breast carcinoma xenografts before and at various time points after injection of the contrast agents at a dose of 0.04 mmol-Gd/kg. The dynamic MR images clearly revealed the contrast enhancement of the agents in the blood, tumor and liver, which could be correlated to the pharmacokinetic profile of the agents. The disulfide bonds were relatively stable initially and strong contrast enhancement with poly(*L*-glutamic acid)-cystamine-(Gd-DO3A) was observed in the blood for at least 60 minutes. Gradual degradation of the spacer in the conjugate then resulted in release of Gd(III) chelates and more rapid blood signal decrease than poly(*L*-glutamic acid)-1,6-hexanediamine-(Gd-DO3A). The contrast enhancement in various organs and tissues could also be viewed in two-dimensional MR images with high spatial resolutions, which showed dynamic and heterogeneous contrast enhancement in tumor tissues. There was no significant difference between the conjugates with different spacers in contrast enhanced tumor imaging.

Targeted MRI contrast agents for the specific detection of molecular biomarkers can be prepared by the incorporating a targeting agent into the polymeric contrast agents. For example, the incorporation of a cyclic RGD peptide into poly(*L*-glutamic acid)-cystamine-(Gd-DO3A) resulted in a targeted MRI contrast agent for the detection of $\alpha_v\beta_3$-integrin, an angiogenesis biomarker [26].

The conjugation of an MRI contrast agent to biomedical polymer can effectively modify its pharmacokinetic properties. The introduction of an extracellular degradable disulfide spacer facilitates the excretion of the Gd(III) chelates in the conjugates. It would be a useful lead to design and develop suitable safe and effective biodegradable macromolecular MRI contrast agents.

2. Non-invasive visualization of in vivo drug delivery of polymer conjugates

The conjugation of anticancer drugs to biomedical polymers modifies their pharmacokinetics and tumor targeting efficiency, resulting in improved therapeutic efficacy. The pharmacokinetics, biodistribution and tumor targeting efficiency of the polymer conjugates are traditionally evaluated using blood and urine sampling, and surgery-based methods. These methods are sometimes invasive and a large number of animals are also required in preclinical studies. Moreover, the pharmacokinetic data obtained with surgical methods cannot accurately reflect true real-time biodistribution in tissues. Molecular imaging provides a non-invasive tool for continuous visualization of pharmacokinetics of polymer drug conjugates in a small number of experimental animals after they are labeled with imaging probes or contrast agents. Non-

invasive visualization has a potential to provide valuable information for understanding the *in vivo* drug delivery mechanisms, which is critical for the design of more efficacious drug delivery systems.

Figure 1 shows that the pharmacokinetics of polymeric MRI contrast agents can be visualized by contrast enhanced MRI, which may also have a potential for noninvasive evaluation of pharmacokinetics of polymer drug conjugates. We have labeled N-(2-hydroxypropyl) methacrylamide copolymers (PHPMA) and poly(*L*-glutamic acid), two of the commonly used carriers for drug delivery, with a stable MRI contrast agent Gd-DO3A to explore the potential [27,28]. The structures of the conjugates are shown in Figure 2 and their physico-chemical characteristics are listed in Table 1. Three different molecular weights with a narrow molecular weight distribution for each conjugate were investigated in athymic nude mice bearing MDA-MB-231 human breast carcinoma xenografts to study the structure and size effect of the conjugates on their pharmacokinetics and tumor targeting efficiency. Three-dimensional MR images of mice were acquired in the same groups of mice before and at various time points after the injection of the conjugates at a dose of 0.03 mmol-Gd/kg. Pharmacokinetics and dynamic biodistribution of the conjugates were clearly visualized in these images.

2.1. MR imaging of PHPMA-GFLG-(Gd-DO3A) conjugates

MR signal intensity indirectly reflects the concentration of the conjugates in the organs or tissues. Bright signal indicates high concentration of the conjugates with similar relaxivities [29]. Strong contrast enhancement was observed in the liver and blood in the heart through the first minute post-injection for all conjugates. The signal gradually faded away depending on the size of the conjugates. Figure 3 shows the representative T_1-weighted coronal MR images of tumor bearing mice, before and at various time points after the injection of the PHPMA-GFLG-(Gd-DO3A) conjugates with three different molecular weights (28, 60 and 120 kDa) at a dose of 0.03 mmol-Gd/kg. Size-dependent pharmacokinetics and biodistribution in blood, major organs and tumor tissues of the conjugates was observed in the dynamic MR images. The low molecular weight conjugate (28 kDa) had a shorter blood circulation time than the conjugates with high molecular weights (60 and 120 kDa). Rapid blood clearance was observed for the 28-kDa conjugate in the MR images. Strong signal in the urinary bladder indicated the excretion of the conjugate via renal filtration. Prolonged blood circulation was seen for the conjugates with higher molecular weights. The 120-kDa conjugate had more prolonged blood circulation than 60-kDa conjugate and was still visible in the blood 72 hours post-injection, while no enhancement was seen for the 60-kDa conjugate. The dynamic MR images also showed that the 60-kDa conjugates was slowly excreted via renal filtration and accumulated in the urinary bladder. Moreover, the dynamic distribution of the conjugates in the liver showed similar size-dependent dynamic patterns as in the blood. The conjugate with higher molecular weight had a higher and more prolonged liver accumulation in the liver. The contrast enhancement in the lung was low as compared to other organs, possibly due to the presence of air.

The MR images revealed size-dependent, dynamic and heterogeneous distribution of the conjugates in tumor tissue, Figure 3. Detailed analysis on 2D spin-echo MR images of the tumor tissues showed that significant contrast enhancement was first observed at the tumor periphery post injection for all conjugates, and then gradually in the tumor interstitium, indicating that the distribution of the conjugates started at the tumor periphery and gradually diffused in the inner tumor tissue [27]. The 28-kDa conjugate had a short blood circulation time and its accumulation was limited to the tumor periphery. The conjugates with higher molecular weights had more prolonged blood circulation and more of the conjugates accumulated in the inner tumor tissue over time than the 28-kDa conjugate. Also, the higher molecular weight conjugate resulted in more significant and prolonged accumulation in the

tumor tissue than the conjugate with a lower molecular weight. The 120-kDa conjugate appears more effective in tumor targeting than the conjugates of lower molecular weights. The 28-kDa conjugate is least effective in tumor targeting among three conjugates. This observation is consistent with the results obtained from conventional pharmacokinetics [30,31], which validates that contrast enhanced MRI is effective for non-invasive evaluation of polymeric drug conjugates. Moreover, contrast enhanced MRI provides detailed information on the dynamic distribution of the conjugates, while conventional pharmacokinetics only provides average distribution data.

2.2. MR imaging of poly(*L*-glutamic acid)-(Gd-DO3A) conjugates

Poly(*L*-glutamic acid) also showed similar size-dependent pharmacokinetics and tumor distribution in contrast enhanced MRI [28]. Figure 4 shows representative T_1-weighted coronal images of mice through the heart, liver and tumor tissue before and at various time points after injection of the conjugates with molecular weight of 28, 60 and 87 kDa. Poly(*L*-glutamic acid) conjugates of high molecular weight had longer blood circulation than the conjugates with low molecular weight. Tumor distribution of the poly(*L*-glutamic acid) conjugates was also heterogeneous. The conjugate of 87 kDa had the longest blood circulation among the conjugates and significant enhancement was still observed at 24 hours post-injection. The longer blood circulation of the poly(*L*-glutamic acid) conjugates with high molecular weights (87 and 60 kDa) resulted in more prolonged accumulation in both tumor periphery and interstitium as compared to the 28-kDa conjugate. The difference between the conjugates with molecular weights of 60 and 87 kDa was not significant based on detailed analysis of signal intensities. Accumulation of the high molecular weight conjugates gradually increased across tumor and remained for a prolonged period.

2.3. Comparison between of HPMA copolymer conjugates and poly(*L*-glutamic acid) conjugates

Contrast enhanced MRI revealed that both HPMA copolymer and poly(*L*-glutamic acid) conjugates showed size dependent pharmacokinetics and tumor targeting efficiency. HPMA copolymers are neutral and non-degradable drug carriers, and poly(*L*-glutamic acid) is an anionic and biodegradable drug carrier. It would be interesting to study the structural effect on pharmacokinetics and tumor targeting efficiency by comparing the polymer conjugates with similar molecular weight distribution. PHPMA-GFLG-(Gd-DO3A) and poly(*L*-glutamic acid)-(Gd-DO3A) with molecular weights of 60 and 28 kDa had similar molecular weight distribution, Figure 5. MR signal intensities in the blood, liver and tumor with these conjugates were analyzed and compared to study the structural effects.

Although MR signal intensity is not linearly correlated to the concentration of the Gd(III) chelates in the conjugates, the comparison of dynamic MR signal intensities of the conjugates would provide qualitative or semi-quantitative information about the structural effect of polymeric conjugates on *in vivo* drug delivery. In order to minimize the variations in different animals caused by MR noise, relative signal intensities were calculated as the ratios of the signal intensities after injection of the conjugates to those before injection in the same regions of interest. High relative signal intensity would represent high concentration of the conjugates.

The dynamic changes of the relative signal intensities in the blood for PHPMA-GFLG-(Gd-DO3A) and poly(*L*-glutamic acid)-(Gd-DO3A) are shown in Figure 6. The HPMA copolymer conjugates showed more prolonged high signal intensities in the blood than poly(*L*-glutamic acid) conjugates of the similar molecular weight distribution or hydrodynamic volume, indicating that HPMA copolymer conjugates had longer blood circulation than the poly(*L*-glutamic acid) conjugates with the same molecular weights. This might be attributed to the fact that poly(*L*-glutamic acid) is biodegradable and *in vivo* degradation of the conjugates may

facilitate its clearance. Although the MRI contrast agent was conjugated to the HPMA copolymer via a degradable tetrapeptide spacer, the spacer was located at side chains and the degradation of the spacer might be much slower than the poly(amino acid) backbone due to steric hindrance. It appears that the non-degradable HPMA copolymer conjugates also had more prolonged liver retention than the poly(L-glutamic acid) conjugates of same molecular weights, Figure 6.

Prolonged blood circulation of the non-degradable HPMA copolymer conjugates resulted in more prolonged high retention in tumor tissues than poly(*L*-glutamic acid) conjugates of the similar molecular weight. Figure 7 shows the dynamic changes of the relative signal intensities of the conjugates in the tumor periphery and interstitium. The 28-kDa HPMA copolymer conjugate demonstrated higher accumulation in both tumor periphery and interstitium than the 28-kDa poly(*L*-glutamic acid) conjugate. The accumulation of both conjugates returned almost to background level at 24 hours post-injection. There was no significant difference in tumor accumulation for the conjugates of 60 kDa in the first 4 hours post-injection. However, the 60-kDa HPMA copolymer conjugate demonstrated much high tumor accumulation at 24 hours post-injection that the 60-kDa poly(glutamic acid) conjugates. These results suggest that the non-degradable HPMA copolymer conjugates may be more effective for tumor targeting than the biodegradable poly(*L*-glutamic acid) conjugates.

These preliminary studies showed that contrast enhanced MRI allows non-invasive visualization of pharmacokinetics of the paramagnetically labeled polymer conjugates with high spatial resolution. Dynamic and heterogeneous distribution of the conjugates in tumor tissue was clearly revealed in the contrast enhanced MR images. As compared to the conventional biopsy-based pharmacokinetic studies, the observations with MRI are made continuously in the same group of experimental animals and the number of animals used is greatly reduced in the study. The observations on the size and structural effect on pharmacokinetics and tumor targeting efficiency of polymer conjugates with contrast enhanced MRI were consistent to what have been reported with conventional pharmacokinetic methods [30,31]. The limitations of contrast enhanced MRI are its low sensitivity and poor accuracy in quantitative measurements of the concentration of contrast agents. MRI technologies such as T_1 and T_2 mapping may provide quantitative measurements. However, currently available quantitative MRI technologies are time consuming and sensitive to motion artifacts, and need further improvements for practical applications. A combination of multiple imaging modalities, including positron emission tomography (PET)-MRI and single photon emission computed tomography (SPECT)-MRI, could provide accurate quantitative assessment of pharmacokinetics and biodistribution with high anatomic resolution for labeled polymer drug conjugates.

3. Bifunctional polymer conjugates for contrast enhanced MRI guided photodynamic therapy

The conjugation of imaging agents or anticancer drugs to biomedical polymers improves their pharmacokinetics and tumor targeting efficiency, resulting in more accurate tumor detection and better therapeutic efficacy. Both imaging agents and anticancer drugs can be loaded onto the same polymer platform to prepare bifunctional conjugates for image-guided therapy. Photodynamic therapy (PDT) is an efficacious modality for cancer treatment [32–33], which involves the administration of a photosensitizer and its activation with light irradiation at the tumor tissue. PDT has been approved for the treatment of malignant diseases, particularly the superficial tumors [34–36]. Treatment of interstitial lesions with photodynamic therapy is limited by the requirement of accurate light irradiation of the target. Bifunctional polymer conjugates containing a photosensitizer drug and an imaging agent will allow accurate

localization of interstitial lesions with diagnostic imaging, which provides guidance for light irradiation to the lesions to achieve specific and maximum therapeutic efficacy.

As shown in previous sections, contrast enhanced MRI with polymeric MRI contrast agents is effective in tumor imaging and allows non-invasive tracking of the tumor accumulation of labeled conjugates. MRI provides high-resolution anatomic images of soft tissues and has been used to guide local destruction of cancerous tissues with ablations, including radiofrequency ablation, thermoablation, cryoablation and laser ablation [37,38]. The combination of contrast enhanced MRI with photodynamic therapy would provide accurate localization of interstitial lesions, guiding specific light irradiation to the tumor tissue in photodynamic therapy. The concept and feasibility of contrast enhanced MRI have been demonstrated by using a bifunctional polymer conjugate containing an MRI contrast agent Gd-(DO3A) and a photosensitizer mesochlorin e_6 (Mce_6), poly-(*L*-glutamic acid)-(Gd-DO3A)-(Mce_6) conjugate [39].

The bifunctional conjugate resulted in significant contrast enhancement in tumor tissue in the athymic nude mice bearing MDA-MB-231 human breast carcinoma xenografts, Figure 8. Poly (*L*-glutamic acid)-(Gd-DO3A) was used as a non-therapeutic control. The gradual and heterogeneous tumor accumulation of the bifunctional conjugates was also visualized by contrast enhanced MRI, which could assist the determination of timing for laser irradiation to achieve the best therapeutic outcome. As shown in the contrast enhanced MR images, high accumulation of the conjugate was observed with first few hours in the tumor periphery, where tissue was highly angiogenic, and the conjugate then gradually diffused into inner tumor tissue.

Two treatment strategies with photodynamic therapy were used based on the dynamic tumor distribution of the conjugate revealed by MRI. The tumor tissues were irradiated with a 650 nm diode laser at 2 hours post-injection to treat the angiogenic tumor tissue when the peripheral vasculature had a relatively high concentration of the conjugate. A second treatment was performed at 18 hours post-injection to further enhance the therapeutic efficacy when more conjugate accumulated in inner tumor tissues. The treatments resulted in higher survival of the mice treated with bifunctional conjugate than those treated with the control. One mouse in the treatment group died 3 days after the treatment for unknown reasons and the rest five mice survived for at least 60 days. Four mice in the control group died within 45 days post-treatment and only two mice survived up to 60 days. Histological studies at the end of experiments demonstrated that the tumor tissue in the treatment group had much lower density of viable cells than those in the control group and the tumor tissues in the control group were more viable than those treated with photodynamic therapy.

Tumor response to the therapy can be non-invasively evaluated by dynamic contrast enhanced MRI with polymeric MRI contrast agents, which can determine physiological properties of tumor tissues based on fractional blood volume and hyperpermeability to macromolecules of tumor blood vessels [40–42]. Vascularity, the density of tumor microvessels, and tumor blood vessel permeability are important parameters for assessing response of tumor tissues to therapies. It has been demonstrated in animal models that dynamic contrast enhanced MRI with macromolecular contrast agents can effectively and non-invasively evaluate tumor response to various therapies [42]. We have shown in a preliminary study that contrast enhanced MRI with a biodegradable macromolecular MRI contrast agent can effectively assess tumor response to photodynamic therapy. The results from dynamic contrast enhanced MRI correlate well with the tumor growth curve after the treatment. The tumors in the treatment group have much lower uptake of the contrast agent than the tumors in the control group.

In summary, the conjugation of anticancer drugs or imaging agent to biomedical polymers modifies their pharmacokinetics and improves their tumor targeting efficiency for more

efficacious cancer treatment and more accurate tumor detection. Molecular imaging provides an effective tool for non-invasive and continuous evaluation of *in vivo* drug delivery of polymer drug conjugates in real time. The combination of drug delivery and molecular imaging on the polymer platform can be used for image-guided therapy. Bifunctional polymer conjugates containing an MRI contrast agent and a photosensitizer are promising for MRI guided photodynamic therapy in cancer treatment. Dynamic contrast enhanced MRI with macromolecular MRI contrast agents has a potential for non-invasive evaluation of tumor responses to therapies. Biocompatible polymers are an effective platform for drug delivery and molecular imaging.

Acknowledgements

The research work is supported in part by NIH grants R21/R33 CA095873, R01 EB000489 and R01 CA097465 and a University of Utah TCP grant.

References

1. Kopecek J, et al. HPMA copolymer-anticancer drug conjugates: design, activity and mechanism of action. Eur J Pharm Biopharm 2000;50:61–81. [PubMed: 10840193]
2. Kobayashi H, Brechbiel MW. Nano-sized MRI contrast agents with dendrimer cores. Adv Drug Deliv Rev 2005 Dec 14;57(15):2271–86. [PubMed: 16290152]
3. Kopecek J, Kopeckova P, Minko T, Lu ZR, Peterson CM. Water soluble polymers in tumor targeted delivery. J Control Release 2001;74:147–58. [PubMed: 11489491]
4. Li C. Poly(L-glutamic acid)--anticancer drug conjugates. Adv Drug Deliv Rev 2002;54:695–713. [PubMed: 12204599]
5. Mohs AM, Lu ZR. Gadolinium(III)-based blood-pool contrast agents for magnetic resonance imaging: status and clinical potential. Expert Opin Drug Deliv 2007;4:149–64. [PubMed: 17335412]
6. Melancon MP, Wang W, Wang Y, Shao R, Ji X, Gelovani JG, Li C. A Novel Method for Imaging In Vivo Degradation of Poly(L-Glutamic Acid), a Biodegradable Drug Carrier. Pharm Res. 2007 Mar 22;Epub ahead of print
7. Raatschen HJ, Fu Y, Shames DM, Wendland MF, Brasch RC. Magnetic resonance imaging enhancement of normal tissues and tumors using macromolecular Gd-based cascade polymer contrast agents: preclinical evaluations. Invest Radiol 2006;41:860–7. [PubMed: 17099424]
8. Zong Y, Guo J, Ke T, Mohs AM, Parker DL, Lu ZR. Effect of size and charge on pharmacokinetics and in vivo MRI contrast enhancement of biodegradable polydisulfide Gd(III) complexes. J Control Release 2006;112:350–6. [PubMed: 16631270]
9. Lu ZR. Application of Biomedical Imaging in Drug Discovery and Development. Pharm Res. 2007Epub ahead of print
10. Rudin M, Weissleder R. Molecular imaging in drug discovery and development. Nat Rev Drug Discov 2003;2:123–31. [PubMed: 12563303]
11. Croy SR, Kwon GS. Polymeric micelles for drug delivery. Curr Pharm Des 2006;12:4669–84. [PubMed: 17168771]
12. Torchilin VP. Micellar nanocarriers: pharmaceutical perspectives. Pharm Res 2007;24:1–16. [PubMed: 17109211]
13. Haider M, Hatefi A, Ghandehari H. Recombinant polymers for cancer gene therapy: a minireview. J Control Release 2005;109:108–19. [PubMed: 16263190]
14. Fu Y, Nitecki DE, Maltby D, Simon GH, Berejnoi K, Raatschen HJ, Yeh BM, Shames DM, Brasch RC. Dendritic iodinated contrast agents with PEG-cores for CT imaging: synthesis and preliminary characterization. Bioconjug Chem 2006 Jul-Aug;17(4):1043–56. [PubMed: 16848414]
15. Mitra A, Coleman T, Borgman M, Nan A, Ghandehari H, Line BR. Polymeric conjugates of mono- and bi-cyclic alphaVbeta3 binding peptides for tumor targeting. J Control Rel 2006;114:175–83.
16. Chen X, Hou Y, Tohme M, Park R, Khankaldyyan V, Gonzales-Gomez I, Bading JR, Laug WE, Conti PS. Pegylated Arg-Gly-Asp peptide: 64Cu labeling and PET imaging of brain tumor alphavbeta3-integrin expression. J Nucl Med 2004;45:1776–83. [PubMed: 15471848]

17. Straub JA, Chickering DE, Church CC, Shah B, Hanlon T, Bernstein H. Porous PLGA microparticles: AI-700, an intravenously administered ultrasound contrast agent for use in echocardiography. J Control Release 2005;108:21–32. [PubMed: 16126299]
18. Kang HW, Weissleder R, Bogdanov A Jr. Targeting of MPEG-protected polyamino acid carrier to human E-selectin in vitro. Amino Acids 2002;23:301–8. [PubMed: 12373551]
19. Liang, Z-P.; Lauterbur, PC. Principles of Magnetic Resonance Imaging. IEEE Press; New York, NY: 2000.
20. Merbach, AE.; Toth, E. The Chemistry of Contrast Agents in Medical Magnetic Resonance Imaging. John Wiley & Sons Ltd; Chichester, England: 2001.
21. Schuhmann-Giampieri G, Schmitt-Willich H, Frezel T, Press WR, Wienmann HJ. In vivo and in vitro evaluation of Gd-DTPA-polylysine as a macromolecular contrast agent for magnetic resonance imaging. Invest Radiol 1991;26:969–974. [PubMed: 1743920]
22. Meyer D, Schaffer M, Chambon C, Beaute S. Paramagnetic dextrans as magnetic resonance blood pool tracers. Invest Radiol 1994;29(Suppl 2):S90–S92. [PubMed: 7523330]
23. Ogan MD, Schmiedl U, Moselely ME, Grodd W, Paajanen H, Brasch RC. Albumin labeled with Gd-DTPA an intravascular contrast-enhancing agent for magnetic resonance blood pool imaging: preparation and characterization. Invest Radiol 1987;22:665–671. [PubMed: 3667174]
24. Lu ZR, Wang X, Parker DL, Goodrich KC, Buswell HR. Poly(l-glutamic acid) Gd(III)- DOTA conjugate with a degradable spacer for magnetic resonance imaging. Bioconjug Chem 2003;14:715–9. [PubMed: 12862423]
25. Ke T, Feng Y, Guo J, Parker DL, Lu ZR. Biodegradable cystamine spacer facilitates the clearance of Gd(III) chelates in poly(glutamic acid) Gd-DO3A conjugates for contrast- enhanced MR imaging. Magn Reson Imaging 2006;24:931–40. [PubMed: 16916710]
26. Ke T, Jeong EK, Wang X, Feng Y, Parker DL, Lu ZR. RGD targeted poly(*L*-glutamic acid)-cystamine-(Gd-DOTA) for MR imaging of angiogenesis. Intl J Nanomed. In press
27. Wang Y, Ye F, Jeong EK, Sun Y, Parker DL, Lu ZR. Noninvasive visualization of pharmacokinetics, biodistribution and tumor targeting of poly[N-(2- hydroxypropyl)methacrylamide] in mice using contrast enhanced. MRI Pharm Res. 2007 Mar 27;
28. Ye F, Ke T, Jeong EK, Wang X, Sun Y, Johnson M, Lu ZR. Noninvasive visualization of in vivo drug delivery of poly(*L*-glutamic acid) using contrast-enhanced MRI. Mol Pharm 2006;3:507–15. [PubMed: 17009849]
29. Zheng J, Liu J, Dunne M, Jaffray DA, Allen C. In Vivo Performance of a liposomal vascular contrast agent for CT and MR-based image guidance applications. Pharm Res. 2007 Mar 21;
30. Veronese FM, Schiavon O, Pasut G, Mendichi R, Andersson L, Tsirk A, Ford J, Wu G, Kneller S, Davies J, Duncan R. PEG-doxorubicin conjugates: influence of polymer structure on drug release, in vitro cytotoxicity, biodistribution, and antitumor activity. Bioconjugate Chem 2005;16:775–784.
31. Seymour LW, Miyamoto Y, Maeda H, Brereton M, Strohalm J, Ulbrich K, Duncan R. Influence of molecular weight on passive tumour accumulation of a soluble macromolecular drug carrier. Eur J Cancer 1995;31A:766–770. [PubMed: 7640051]
32. Dougherty TJ, Gomer CJ, Henderson BW, Jori G, Kessel D, Korbelik M, Moan J, Peng Q. Photodynamic therapy. J Natl Cancer Inst 1998;90:889–905. [PubMed: 9637138]
33. Huang Z. A review of progress in clinical photodynamic therapy. Technol Cancer Res Treat 2005;4:283–93. [PubMed: 15896084]
34. Dolmans DE, Fukumura D, Jain RK. Photodynamic therapy for cancer. Nat Rev Cancer 2003;3:380–387. [PubMed: 12724736]
35. Kormeili T, Yamauchi PS, Lowe NJ. Topical photodynamic therapy in clinical dermatology. Br J Dermatol 2004;150:1061–1069. [PubMed: 15214890]
36. Hopper C, Kubler A, Lewis H, Tan IB, Putnam G. mTHPC-mediated photodynamic therapy for early oral squamous cell carcinoma. Int J Cancer 2004;111:138–146. [PubMed: 15185355]
37. Frich L, Bjormerud A, Fossheim S, Tillung T, Gladhaug I. Experimental application of thermosensitive paramagnetic liposomes for monitoring magnetic resonance imaging guided thermal ablation. Magn Reson Med 2004;52:1302–1309. [PubMed: 15562487]

38. Dichfeld T, Calkins H, Zviman M, Kato R, Meininger G, Lickfelt L, Berger R, Halperin H, Soloman SB. Anatomic stereotactic catheter ablation on three-dimensional magnetic resonance images in real time. Circulation 2003;108:2407–2413. [PubMed: 14568905]

39. Vaidya A, Sun Y, Ke T, Jeong EK, Lu ZR. Contrast enhanced MRI-guided photodynamic therapy for site-specific cancer treatment. Magn Reson Med 2006;56:761–7. [PubMed: 16902981]

40. Jordan BF, Runquist M, Raghunand N, Baker A, Williams R, Kirkpatrick L, Powis G, Gillies RJ. Dynamic contrast-enhanced and diffusion MRI show rapid and dramatic changes in tumor microenvironment in response to inhibition of HIF-1alpha using PX- 478. Neoplasia 2005;7:475–85. [PubMed: 15967100]

41. Wilmes LJ, Pallavicini MG, Fleming LM, Gibbs J, Wang D, Li KL, Partridge SC, Henry RG, Shalinsky DR, Hu-Lowe D, Park JW, McShane TM, Lu Y, Brasch RC, Hylton NM. AG-013736, a novel inhibitor of VEGF receptor tyrosine kinases, inhibits breast cancer growth and decreases vascular permeability as detected by dynamic contrast-enhanced magnetic resonance imaging. Magn Reson Imaging 2007;25:319–27. [PubMed: 17371720]

42. Preda A, van Vliet M, Krestin GP, Brasch RC, van Dijke CF. Magnetic resonance macromolecular agents for monitoring tumor microvessels and angiogenesis inhibition. Invest Radiol 2006;41:325–31. [PubMed: 16481916]

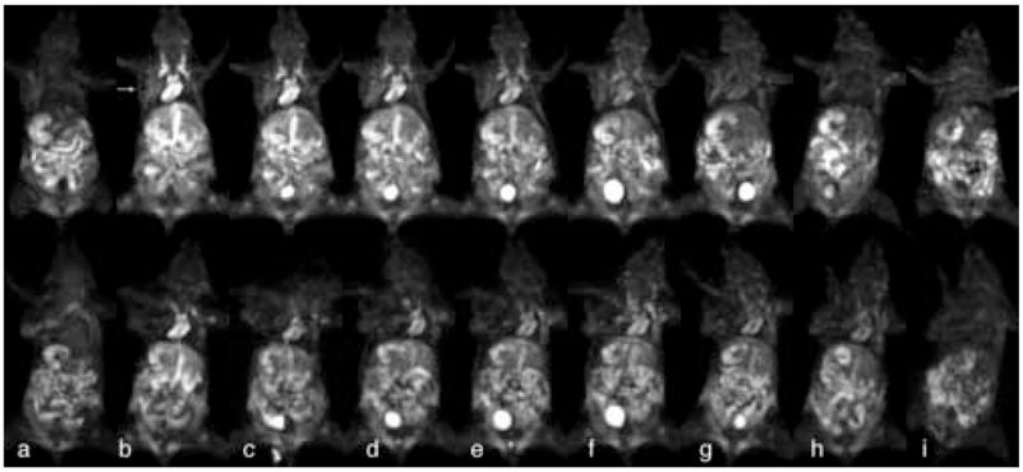

Figure 1.
Contrast enhanced 3D (MIP) MR images of mice bearing tumors using PGA-cystamine-(Gd-DO3A) (top) and PGA-1,6-diaminohexane-(Gd-DO3A) (bottom) at a dose of 0.04 mmol-Gd/kg. The images were taken before contrast (a), and 5 (b), 15 (c), 30 min (d), 1 (e), 2 (f), 4 (g), 7 (h), and 24 h (i) postinjection. Arrow points to tumor.

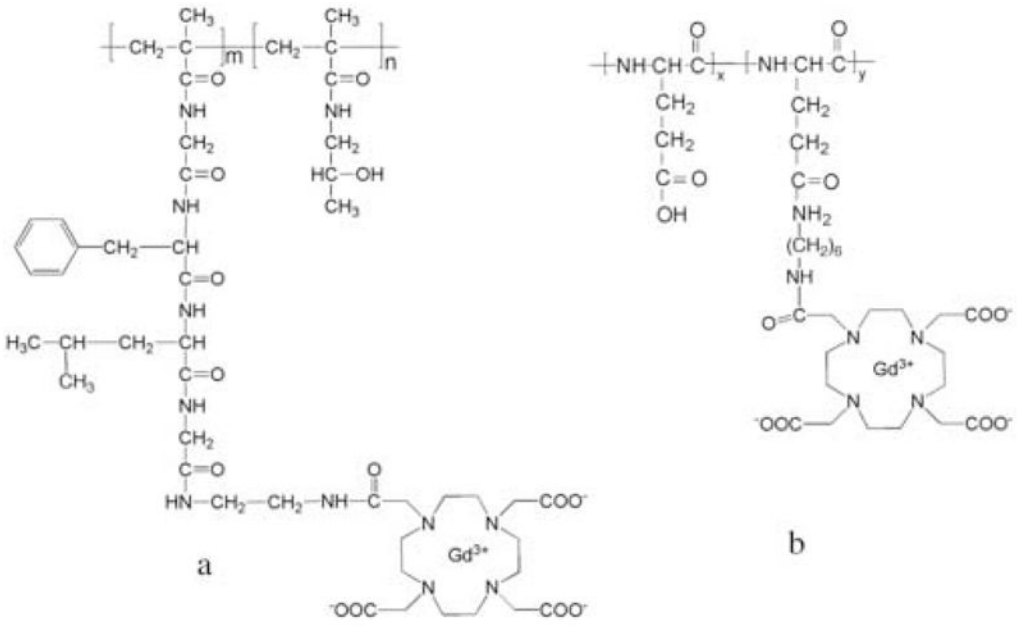

Figure 2.
The chemical structures of PHPMA-GFLG-(Gd-DO3A) (a) and poly(*L*-glutamic acid)-(Gd-DO3A) (b) conjugates.

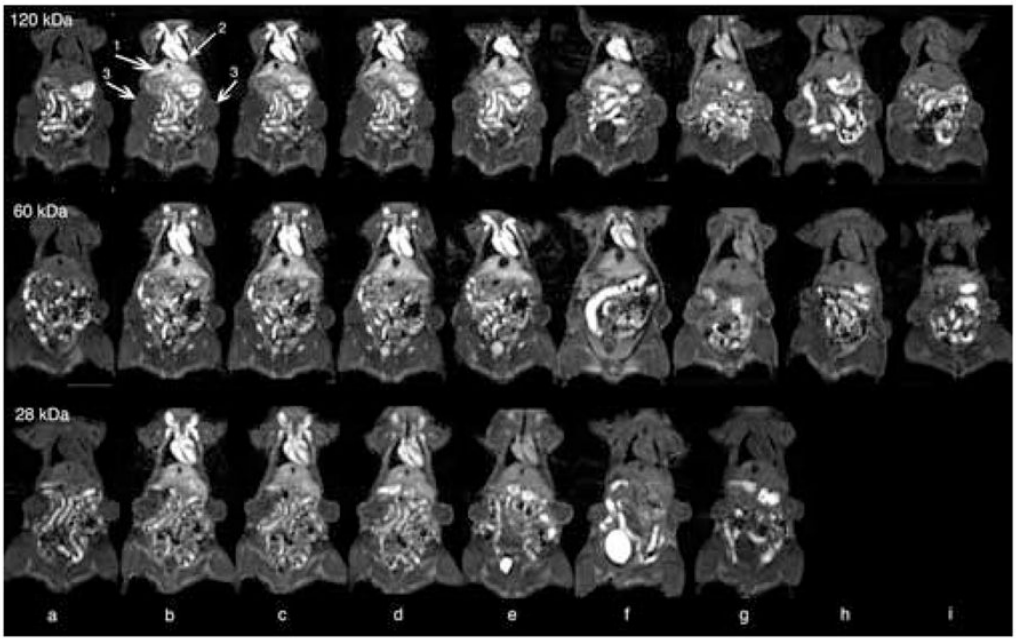

Figure 3.
Coronal MR images of mice injected with PHPMA-GFLG-(Gd-DO3A) (GFLG) conjugates with molecular weights of 28, 60 and 120 kDa before contrast (a) and at 1 min (b), 10 min (c), 20 min (d), 1 hour (e), 4 hour (f), 24 hour (g), 48 hour (h), and 72 hour (i) after the injection of the conjugates at a dose of 0.03 mmol-Gd/kg. The arrows point to the heart (1), liver (2) and tumor (3).

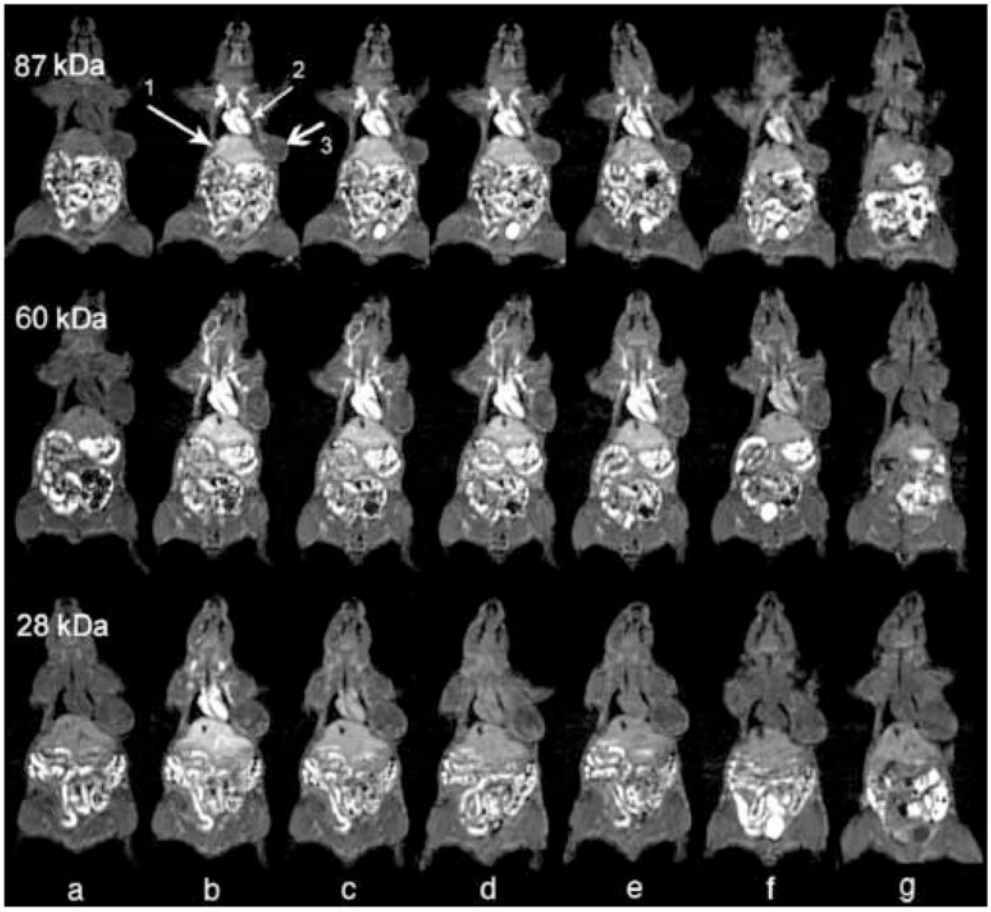

Figure 4.

Coronal MR images of mice injected with poly(*L*-glutamic acid)-(Gd-DO3A) conjugates with molecular weights of 28, 60 and 87 kDa before contrast (a) and at 1 min (b), 10 min (c), 20 min (d), 1 hour (e), 4 hour (f), and 24 hour (g) after the injection of the conjugates at a dose of 0.03 mmol-Gd/kg. The arrows point to the heart (1), liver (2) and tumor (3).

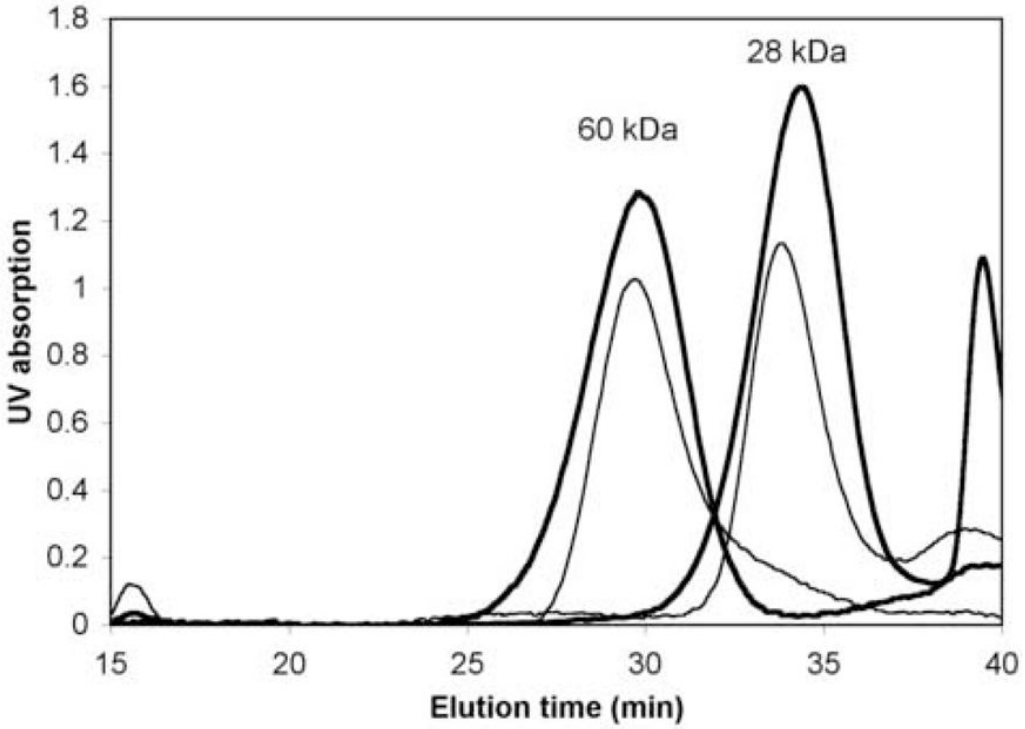

Figure 5.
Size exclusion chromatograms of PHPMA-GFLG-(Gd-DO3A) (thick lines) and poly(*L*-glutamic acid)-(Gd-DO3A) (thin lines) conjugates.

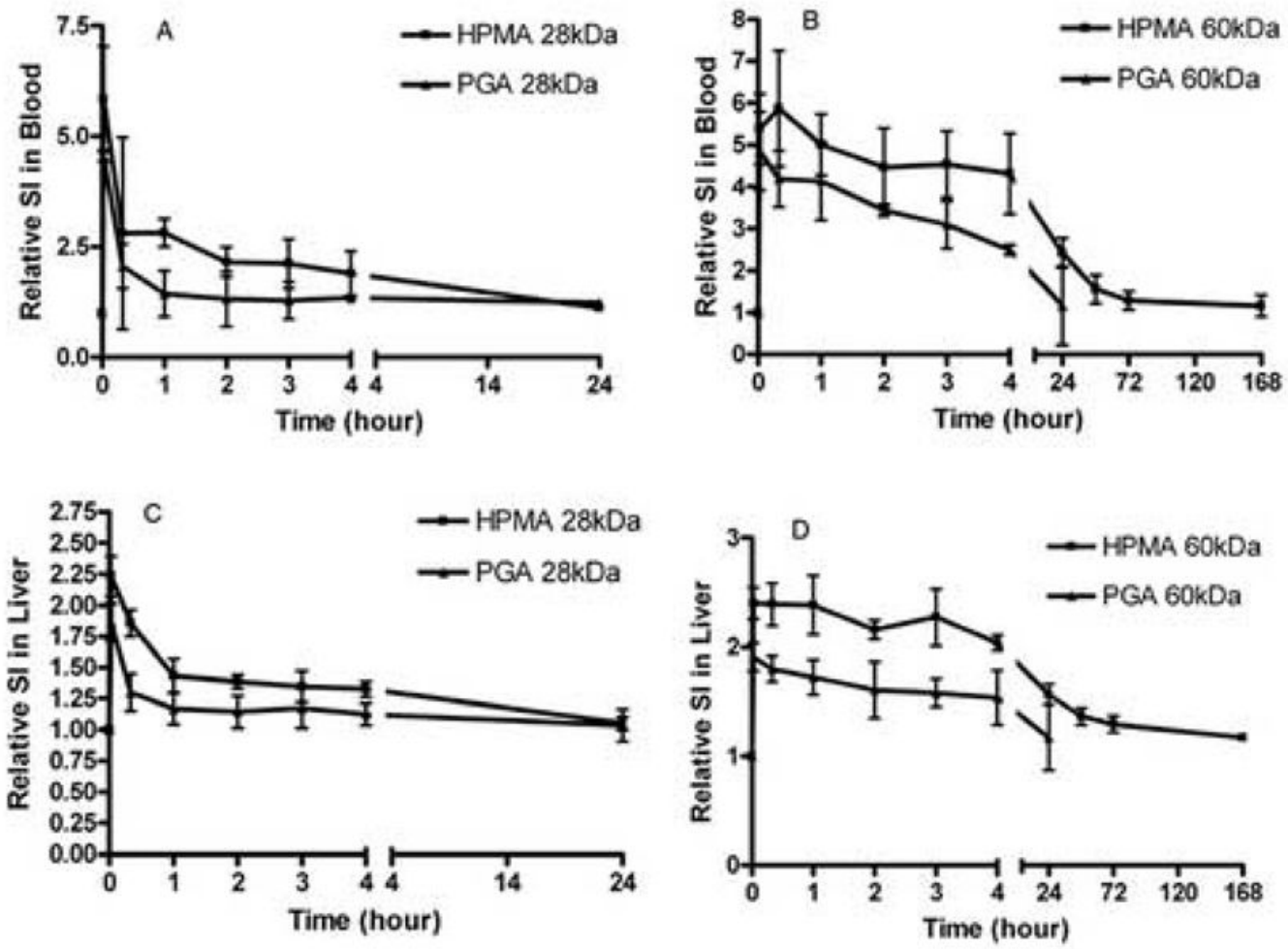

Figure 6.

Relative signal intensities (SI) of the PHPMA-GFLG-(Gd-DO3A) and poly(L-glutamic acid)-(Gd-DO3A) conjugates in the blood (28 kDa, A and 60 kDa, B) and the liver (28 kDa, C and 60 kDa, D) at various time points after the injection of the conjugates at a dose of 0.03 mmol-Gd/kg.

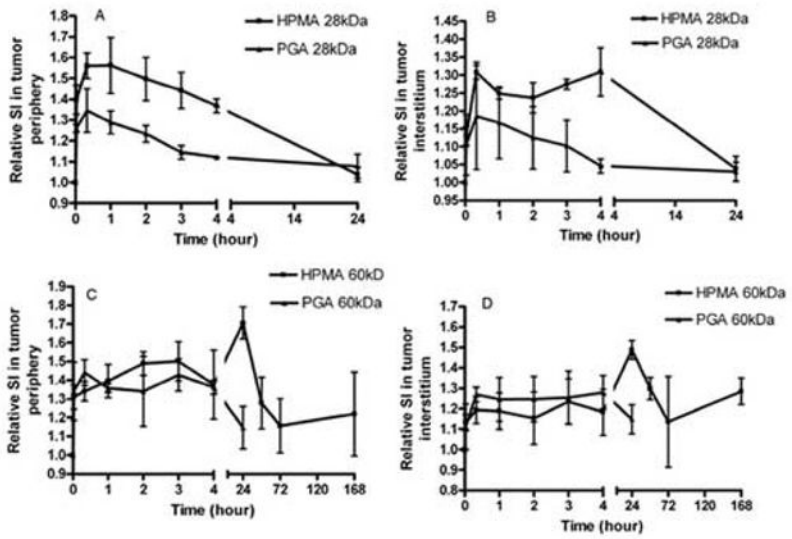

Figure 7.

Relative signal intensities (SI) of the PHPMA-GFLG-(Gd-DO3A) and poly(L-glutamic acid)-(Gd-DO3A) conjugates in the tumor periphery (28 kDa, A and 60 kDa, C) and interstitium (28 kDa, B and 60 kDa, D) at various time points after the injection of the conjugates at a dose of 0.03 mmol-Gd/kg.

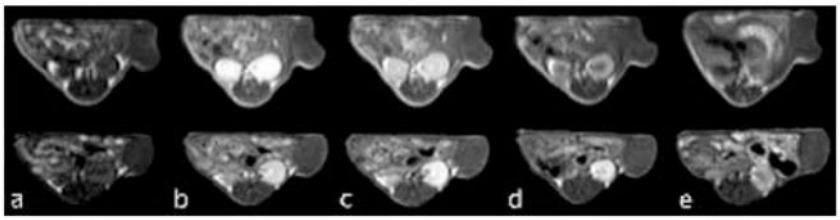

Figure 8.

Representative 2D Spin echo images of tumors in mice receiving 0.05-mmol Gd^{3+}/kg PGA-(Gd-DO3A)-Mce_6 (top panel), PGA-(Gd-DO3A)-Mce_6 (lower panel), and PGA-(Gd-DO3A) (bottom panel) before (a) and at 2min (b), 30 min (c), 2 hours (d), and 18 hours (e) post injection.

Table 1

Physicochemical Characteristics of PHPMA-GFLG-DO3A Conjugates and Poly(L-glutamic acid)-DO3A Conjugates

PGA-Gd-DO3A	**PHPMA-GFLG-Gd-DO3A**					
	PGA-28	**PGA-60**	**PGA-87**	**GFLG-28**	**GFLG-60**	**GFLG-120**
Gd-content (mmol/g)	0.40	0.42	0.55	0.36	0.37	0.39
T_1 relaxivity ($mM^{-1}s^{-1}$)	9.19	9.44	9.45	11.9	10.9	11.5
M_w (KDa)	28.0	60.0	87.0	28.0	59.5	120
M_n (KDa)	26.9	54.5	60.0	25.9	55.6	115